The Astrophysical Journal, 823:7 (11pp), 2016 May 20 doi:10.3847/0004-637X/823/1/7

ION DYNAMICS AT A RIPPLED QUASI-PARALLEL SHOCK: 2D HYBRID SIMULATIONS

Yufei Hao[1,2], Quanming Lu[1,2], Xinliang Gao[1,2], and Shui Wang[1,2]
[1] CAS Key Laboratory of Geospace Environment, Department of Geophysics and Planetary Science, University of Science and Technology of China, Hefei 230026, China; qmlu@ustc.edu.cn
[2] Collaborative Innovation Center of Astronautical Science and Technology, China
Received 2016 February 4; accepted 2016 March 5; published 2016 May 16

ABSTRACT

In this paper, two-dimensional hybrid simulations are performed to investigate ion dynamics at a rippled quasi-parallel shock. The results show that the ripples around the shock front are inherent structures of a quasi-parallel shock, and the re-formation of the shock is not synchronous along the surface of the shock front. By following the trajectories of the upstream ions, we find that these ions behave differently when they interact with the shock front at different positions along the shock surface. The upstream particles are transmitted more easily through the upper part of a ripple, and the corresponding bulk velocity downstream is larger, where a high-speed jet is formed. In the lower part of the ripple, the upstream particles tend to be reflected by the shock. Ions reflected by the shock may suffer multiple-stage acceleration when moving along the shock surface or trapped between the upstream waves and the shock front. Finally, these ions may escape further upstream or move downstream; therefore, superthermal ions can be found both upstream and downstream.

Key words: acceleration of particles – shock waves

Supporting material: animations

1. INTRODUCTION

In a quasi-parallel shock, the angle between the upstream background magnetic field and the shock normal (θ_{Bn}) is smaller than 45° (Jones & Ellison 1991). Such a peculiar property allows ions reflected by a supercritical quasi-parallel shock to travel far upstream along the magnetic field, and the resulting plasma beam instabilities can excite various large-amplitude low-frequency waves (Fairfield 1969; Russell & Hoppe 1983; Gary et al. 1984; Lin 2003; Eastwood et al. 2004; Blanco-Cano et al. 2009, 2011; Omidi et al. 2013; Wilson et al. 2013; Wu et al. 2015). These waves are then brought back by the upstream plasma toward the shock front. In such a process, the waves begin to steepen and the amplitude is enhanced when they approach the shock front, and finally a new shock front is formed after the waves interact and merge with the former shock front (Burgess 1989; Thomas et al. 1990; Winske et al. 1990; Schwartz & Burgess 1991; Scholer & Burgess 1992; Schwartz et al. 1992; Scholer et al. 1993; Su et al. 2012a, 2012b). These large-amplitude waves play an important role in diffusive shock acceleration (DSA) by scattering the reflected ions across a quasi-parallel shock many times, while DSA is the mechanism responsible for almost universally observed power-law spectra of energetic particles from cosmic rays to gradual solar energetic particle events (Axford et al. 1977; Bell 1978; Blandford & Ostriker 1978; Lee 1983; Zank et al. 2000; Giacalone 2003; Li et al. 2003; Zuo et al. 2013; Cui et al. 2015). However, for a particle to be accelerated at a shock by the DSA mechanism, the particle must be sufficiently energetic to become a seed particle of DSA so that it can be scattered across all the micro- and macrostructures of the shock many times—this is the well known "injection problem" (Jokipii 1987; Zank et al. 2001; Scholer et al. 2002; Su et al. 2012a; Caprioli et al. 2015; Johlander et al. 2016).

How thermal ions upstream of a quasi-parallel shock become superthermal ions and then provide the seed particles for further acceleration by DSA has been thoroughly investigated with hybrid simulations by several authors (Scholer 1990; Kucharek & Scholer 1991; Scholer & Burgess 1992; Su et al. 2012a, 2012b; Guo & Giacalone 2013). The superthermal ions at a quasi-parallel shock come from the ions reflected by the shock after they stay close to the shock front and are accelerated for an extended period of time (Scholer 1990; Guo & Giacalone 2013). Such a process is considered as the initial state of DSA, and these ions provide the seed particles for further acceleration by DSA (Scholer & Burgess 1992; Su et al. 2012a; Guo & Giacalone 2013). Kucharek & Scholer (1991) further found that the acceleration from the reflected ions to the superthermal ions is mainly due to grad B drift around the shock front. Su et al. (2012a, 2012b) pointed out that the extended stay of these reflected ions close to the shock front results from trapping between the new and old shock fronts during the re-formation of the quasi-parallel shock. These ions are accelerated every time when they are reflected by the new shock front, and finally they escape upstream and become superthermal ions after the re-formation cycle of the shock is finished. These superthermal ions can be accelerated out of the core part as well as the outer part of the velocity space of the incident upstream plasma. The other reflected ions will return to the shock immediately and then be transmitted downstream quickly, and these ions lead to ion heating downstream.

However, a 1D hybrid simulation model cannot take into account the influence of the structures along the shock surface on ion dynamics. Recently, ripples with local curvature variations around the shock front have been found to be inherent structures of a quasi-parallel shock, which causes fast, deflected jets downstream (Hietala et al. 2009; Hietala & Plaschke 2013). The characteristics of such high-speed jets downstream of a quasi-parallel shock have already been identified by satellite observations in the Earth's bow shock (Němeček et al. 1998; Savin et al. 2012; Hietala et al. 2009, 2012; Archer et al. 2012; Plaschke et al. 2013). In this paper, we investigate ion dynamics at a rippled quasi-parallel shock

by performing a two-dimensional (2D) hybrid simulation, and the effects of the ripples on both the reflected and transmitted ions are considered.

In this paper, we first describe the simulation model in Section 2; the simulation results are presented in Section 3, and discussed and summarized in Section 4.

2. SIMULATION MODEL

A 2D hybrid simulation is performed in this paper to investigate ion dynamics at a rippled quasi-parallel shock. A hybrid simulation model treats ions as macroparticles, and their motions are governed by

$$m_p \frac{d\boldsymbol{v}_p}{dt} = e\left(\boldsymbol{E} + \frac{\boldsymbol{v}_p \times \boldsymbol{B}}{c}\right) - e\eta \boldsymbol{J} \quad (1)$$

where v_p is the ion velocity and m_p is its mass. E, B, and J represent the electric field, magnetic field, and current, respectively. η is the resistivity resulting from the interaction between particles and high-frequency waves. Electrons are treated as a massless fluid, and the momentum equation is

$$-en_e\left(\boldsymbol{E} + \frac{\boldsymbol{V}_e \times \boldsymbol{B}}{c}\right) - \nabla p_e + en_e\eta \boldsymbol{J} = \frac{\partial}{\partial t}(n_e m_e \boldsymbol{V}_e) = 0.$$

Therefore,

$$\boldsymbol{E} = -\frac{\boldsymbol{V}_e \times \boldsymbol{B}}{c} - \frac{\nabla p_e}{n_e e} + \eta \boldsymbol{J} \quad (2)$$

where $\boldsymbol{V}_e$ is the bulk velocity of electrons and n_e is their number density. The electron pressure is expressed as $p_e = n_e k T_e$, where T_e is the electron temperature and k is the Boltzmann constant.

Charge neutrality is assumed in the hybrid simulation model. Then, $n_e = n_p = \int f(\boldsymbol{v}_p) d^3\boldsymbol{v}_p = n$, where n_p is the number density of ions and $f(\boldsymbol{v}_p)$ is their velocity distribution, which can be obtained after we know the positions and velocities of all particles. The current can be calculated with Ampère's law,

$$\frac{4\pi}{c}\boldsymbol{J} = \nabla \times \boldsymbol{B}. \quad (3)$$

Then, we can know the bulk velocity of electrons from the current (J) and the bulk velocity of ions ($\boldsymbol{V}_p$, where $\boldsymbol{V}_p = \int \boldsymbol{v}_p f(\boldsymbol{v}_p) d^3\boldsymbol{v}_p$) according to the equation $J = ne(\boldsymbol{V}_p - \boldsymbol{V}_e)$.

The magnetic field can be calculated from Faraday's law:

$$\frac{1}{c}\frac{\partial \boldsymbol{B}}{\partial t} = -\nabla \times \boldsymbol{E} \quad (4)$$

and

$$\nabla \cdot \boldsymbol{B} = 0. \quad (5)$$

Besides Equations (1)–(5), we still need the equation of state of the electrons, which is assumed to be adiabatic, to implement the algorithm of the hybrid simulation model; the details can be found in Winske (1985).

Initially, plasma with a fixed bulk velocity ($V_{\rm inj} = 4.5V_A$, where V_A is the upstream Alfvén speed) moves to the right rigid boundary, and the background magnetic field B_0 lies in the x–y plane. The plasma is reflected when it reaches the right boundary and interacts with continuously injected plasma, and this interaction leads to the formation of a shock front. Meanwhile, the shock front has a propagation velocity pointing to the left

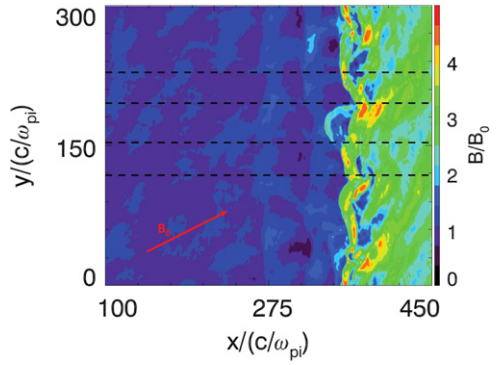

Figure 1. The total magnetic field at $\Omega_i t = 125$. The dashed lines denote four cuts along $y = 118$, 153, 195, and $228c/\omega_{\rm pi}$. The red arrow indicates the direction of the upstream magnetic field.

along the x direction, which is the global shock normal. A periodic boundary condition is used in the y direction. For the shock in this simulation, $\theta_{\rm Bn}$ (the angle between the shock normal and the direction of upstream background magnetic field) is 30°, and the upstream plasma beta is $\beta_p = \beta_e = 0.4$ (where p and e indicate proton and electron, respectively). The velocity of the shock in the downstream reference frame is about $1.0V_A$, and then the Mach number is around 5.5, which is a typical value for a terrestrial bow shock. The simulation plane covers an area of length $L_x = n_x \times \Delta x = 1000 \times 0.5c/\omega_{\rm pi} = 500c/\omega_{\rm pi}$ and width $L_y = n_y \times \Delta y = 300 \times 1.0c/\omega_{\rm pi} = 300c/\omega_{\rm pi}$ (where n_x and n_y are the numbers of grid cell, Δx and Δy are grid sizes, c is the speed of light, and $\omega_{\rm pi}$ is the ion plasma frequency under upstream parameters). The electron resistive length ($L_\eta = \eta c^2/(4\pi V_A)$, where η denotes the wave–particle effects resulting from high-frequency plasma instabilities) is set to be $L_\eta = 0.1$, which is much smaller than the grid size. The time step is $\Delta t = 0.02\Omega_i^{-1}$ (where $\Omega_i = eB_0/m$ is the ion gyrofrequency).

3. SIMULATION RESULTS

Ripples with the local curvature variations around the shock front are inherent structures of a quasi-parallel shock, and they can be seen clearly in Figure 1, which plots the total magnetic field at $\Omega_i t = 125$. The shock front is around $x = 364c/\omega_{\rm pi}$, where obvious ripples with a size of about 75 $c/\omega_{\rm pi}$ can be found along the y direction. Here the position of the shock is calculated as follows: we average the magnetic field along the y direction and obtain a one-dimensional shock, and at such a one-dimensional shock the total magnetic field has its maximum gradient at the position of the shock. Plasma waves with amplitude $\delta B/B_0 \sim 1$ and wavelength about $50c/\omega_{\rm pi}$ exist upstream. These waves have also been identified in previous simulations (Scholer & Burgess 1992; Scholer et al. 1993; Scholer 1993; Blanco-Cano et al. 2009; Su et al. 2012a, 2012b), and they correspond to the reported ultralow-frequency (ULF) waves in satellite observations (Schwartz et al. 1992; Burgess et al. 2005; Lucek et al. 2008; Eastwood et al. 2005a, 2005b; Wu et al. 2015). The amplitude of these waves will become large as they approach the shock front, and finally a new shock front may be generated. Such a re-formation of the shock can be demonstrated more clearly in Figure 2, which shows the time evolution of the total magnetic field along (a) $y = 118c/\omega_{\rm pi}$, (b) $y = 153c/\omega_{\rm pi}$, (c) $y = 195c/\omega_{\rm pi}$, and (d) $y = 228c/\omega_{\rm pi}$, as denoted by the dashed lines in Figure 1. The period of the shock

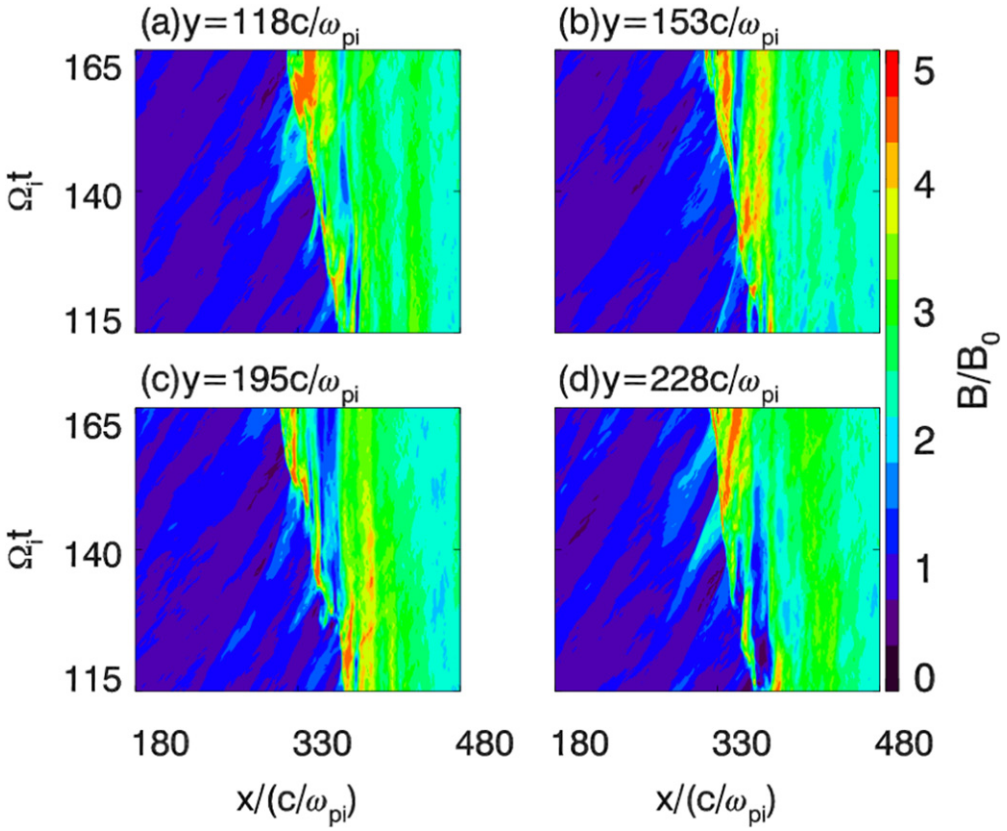

Figure 2. The evolution of the total magnetic field along (a) $y = 118c/\omega_{\rm pi}$, (b) $y = 153c/\omega_{\rm pi}$, (c) $y = 195c/\omega_{\rm pi}$, (d) $y = 228c/\omega_{\rm pi}$, which have been denoted by dashed lines in Figure 1.

re-formation is about $25\Omega_i^{-1}$. Due to the existence of the ripples around the shock front, the re-formation is not synchronous at different y positions.

By following a group of ions, we can investigate ion dynamics at the rippled quasi-parallel shock. These particles are located in the areas ($320c/\omega_{\rm pi} \leqslant x \leqslant 370c/\omega_{\rm pi}$, $114c/\omega_{\rm pi} \leqslant y \leqslant 141c/\omega_{\rm pi}$) and ($320c/\omega_{\rm pi} \leqslant x \leqslant 380c/\omega_{\rm pi}$, $168c/\omega_{\rm pi} \leqslant y \leqslant 198c/\omega_{\rm pi}$) at $\Omega_i t = 121.5$, which are denoted by "A" and "B" in Figure 3. At $\Omega_i t = 121.5$, these particles just begin to interact with the shock front. The particles in region "A" interact with the lower part of one selected ripple, while the particles in region "B" interact with the upper part of the same ripple. Figures 4 and 5 respectively plot the evolution of the ions in regions "A" and "B" (these particles at $\Omega_i t = 121.5$ are restricted to the regions "A" and "B" denoted by the red boxes in Figure 3) at four different times $\Omega_i t = 121.5$, 161.5, 171.5, and $\Omega_i t = 181.5$. In each figure, the left column represents the positions of particles (the magnetic field is also plotted for reference), the middle column describes the corresponding velocity distribution ($v = \sqrt{v_x^2 + v_y^2 + v_z^2}$), and the right column presents the distribution of the ion velocity in the x direction (v_x). In the left column, the red particles mean that these particles are located upstream of the shock, and the position of the shock front is indicated by the red dashed lines, which are located at $x = 338c/\omega_{\rm pi}$, $348c/\omega_{\rm pi}$, and $358c/\omega_{\rm pi}$ at $\Omega_i t = 161.5$, $\Omega_i t = 171.5$, and $\Omega_i t = 181.5$, respectively (the position of the shock is calculated with the method described in Figure 1). In the middle and right columns, the red area shows the percentage of the particles located upstream of the shock. At $\Omega_i t = 121.5$, the particles

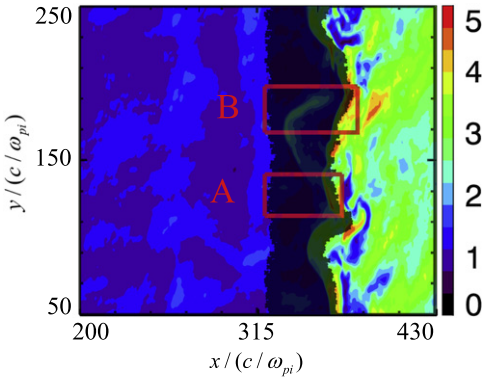

Figure 3. The position of the selected ions at $\Omega_i t = 121.5$, which are restricted in the area ($250 \leqslant x \leqslant 270$, $0 \leqslant y \leqslant 300$) at $\Omega_i t = 100$. The boxes "A" and "B" denote the areas ($310c/\omega_{\rm pi} \leqslant x \leqslant 370c/\omega_{\rm pi}$, $114c/\omega_{\rm pi} \leqslant y \leqslant 141c/\omega_{\rm pi}$) and ($315c/\omega_{\rm pi} \leqslant x \leqslant 380c/\omega_{\rm pi}$, $168c/\omega_{\rm pi} \leqslant y \leqslant 198c/\omega_{\rm pi}$), respectively.

begin to interact with the shock, and the interaction lasts for a time of about $4.5\Omega_i^{-1}$ (the interaction time is the time period from the moment when the particles just begin to interact with the shock to the moment when the interaction almost finishes), which is much smaller than the period of shock re-formation ($\sim 25\Omega_i^{-1}$). Therefore, during the interaction between the particles and shock, the shock can be considered as stationary. After the interaction, the particles can be separated into two parts: the particles transmitted downstream and the others remaining upstream, and both these groups of particles almost move along the magnetic field. Obviously, the ions in region "A" (in the lower part of the ripple) are reflected more easily by the shock. As shown in the right column of each figure, the

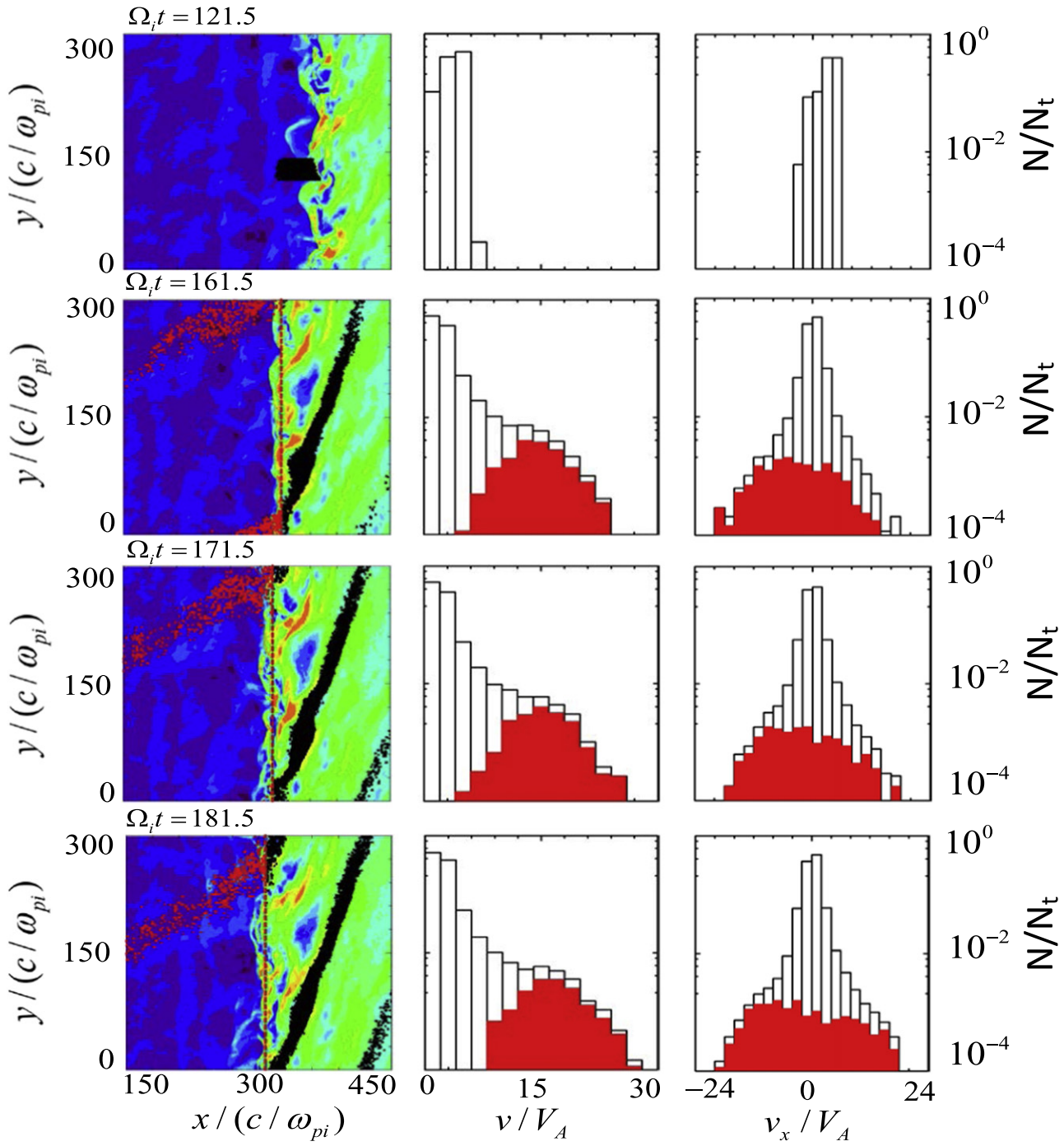

Figure 4. The time evolution of the particles in areas "A" at $\Omega_i t = 121.5$, 161.5, 171.5, and 181.5. The particles at $\Omega_i t = 121.5$ are restricted to area "A," which has been indicated in Figure 3. The left column represents the positions of particles (the magnetic fields are plotted for reference), and the red particles mean that these particles are located upstream of the shock. The position of shock front is indicated by the red dashed line in the left column, and is at $338c/\omega_{\rm pi}$, $348c/\omega_{\rm pi}$, and $358c/\omega_{\rm pi}$ at $\Omega_i t = 161.5$, $\Omega_i t = 171.5$, and $\Omega_i t = 181.5$, respectively. The middle column plots the corresponding velocity distribution ($v = \sqrt{v_x^2 + v_y^2 + v_z^2}$, where N_t is the total number of particles and N is the number in a definite velocity range) and the right column shows the distribution of ion velocity in the x direction (v_x). The red area shows the percentage of particles located upstream of the shock.

particles remaining upstream can have either negative v_x or positive v_x, which means that they can move upstream or downstream of the shock. The reason why the particles remaining upstream can move downstream is due to the scattering of the upstream waves, as discussed in the following by tracing the trajectories of several typical ions. Finally, for the particles from region "A," the particles remaining upstream comprise about 1.48% of the total particles. For the particles from region "B," the percentage of particles remaining upstream is about 0.22%. In region "A," the local shock can be considered as a quasi-parallel shock because the local shock angle (the angle between the local shock normal and upstream magnetic field) is less than 45°, and the upstream particles are reflected by the shock more efficiently and escape more easily upstream. In region "B," the local shock is more like a quasi-perpendicular shock, and it is more difficult for the upstream

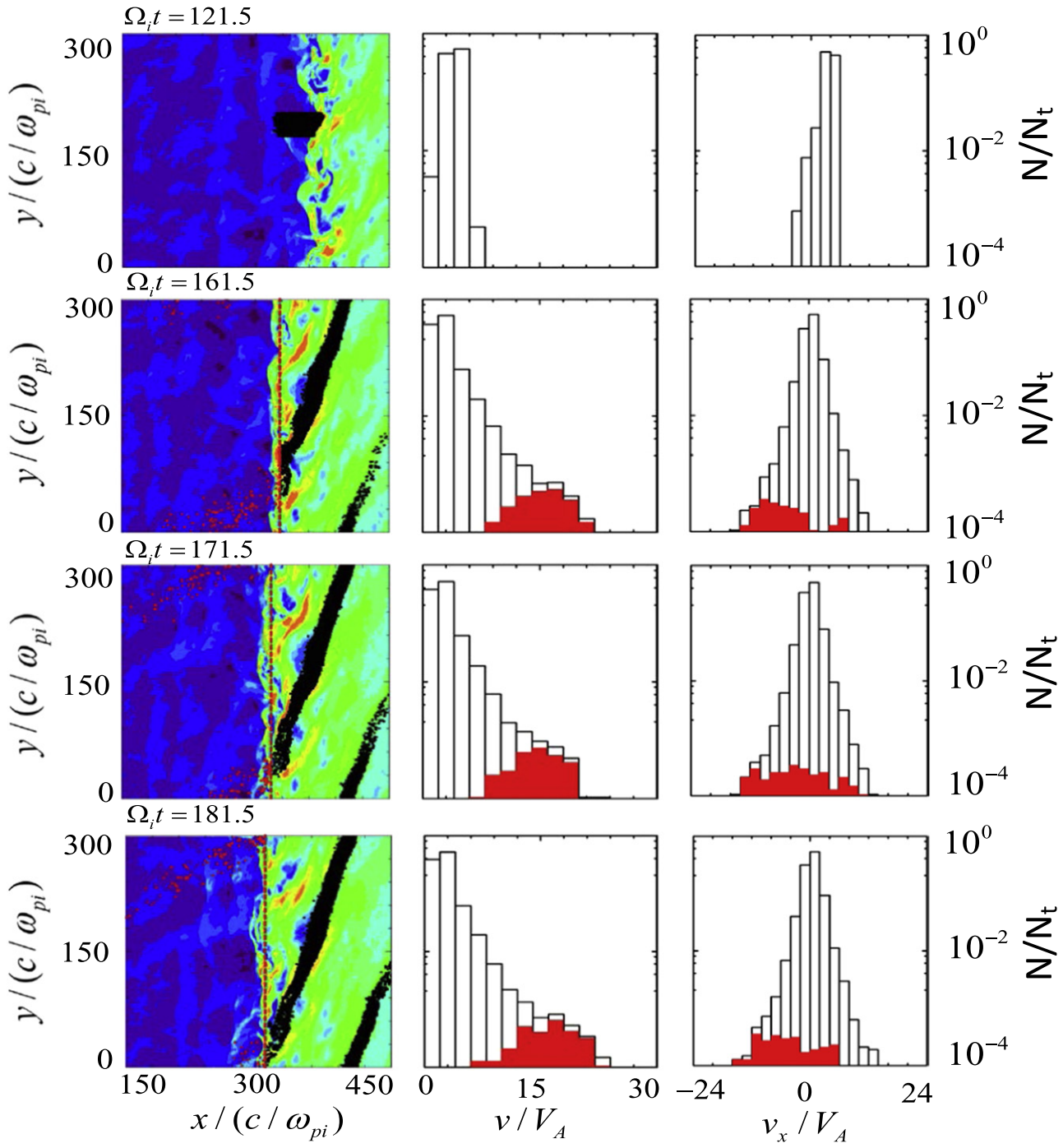

Figure 5. The time evolution of the particles in areas "B" at $\Omega_i t = 121.5$, 161.5, 171.5, and 181.5. The particles at $\Omega_i t = 121.5$ are restricted to area "B," which has been indicated in Figure 3. The left column represents the positions of particles (the magnetic fields are plotted for reference), and the red particles mean that these particles are located upstream of the shock. The position of shock front is indicated by the red dashed line in the left column, and is at $338c/\omega_{\rm pi}$, $348c/\omega_{\rm pi}$, and $358c/\omega_{\rm pi}$ at $\Omega_i t = 161.5$, $\Omega_i t = 171.5$, and $\Omega_i t = 181.5$, respectively. The middle column plots the corresponding velocity distribution ($v = \sqrt{v_x^2 + v_y^2 + v_z^2}$, where N_t is the total number of particles and N is the number in a definite velocity range) and the right column shows the distribution of the ion velocity in the x direction (v_x). The red area shows the percentage of particles located upstream of the shock.

particles to be reflected and escape upstream. From the velocity distribution of particles, we can find that the ions are highly accelerated with a maximum velocity $\sim 30 V_A$ after they interact with the shock. Although most of the superthermal ions come from the ions remaining upstream after they interact with the shock, we can still find that some of the superthermal ions come from downstream. This is different from the 1D hybrid simulation results for a quasi-parallel shock (Su et al. 2012a), where all the superthermal ions come from upstream, and this will be demonstrated in the following by tracing the trajectories of several typical ions. It is also no surprise that there are more superthermal ions from region "A" than from region "B," because the local shock in region "A" is more like a quasi-parallel shock. For the particles transmittted downstream, the bulk velocity of the particles from region "B" is larger than that of the particles from region "A." Therefore, the lower part of

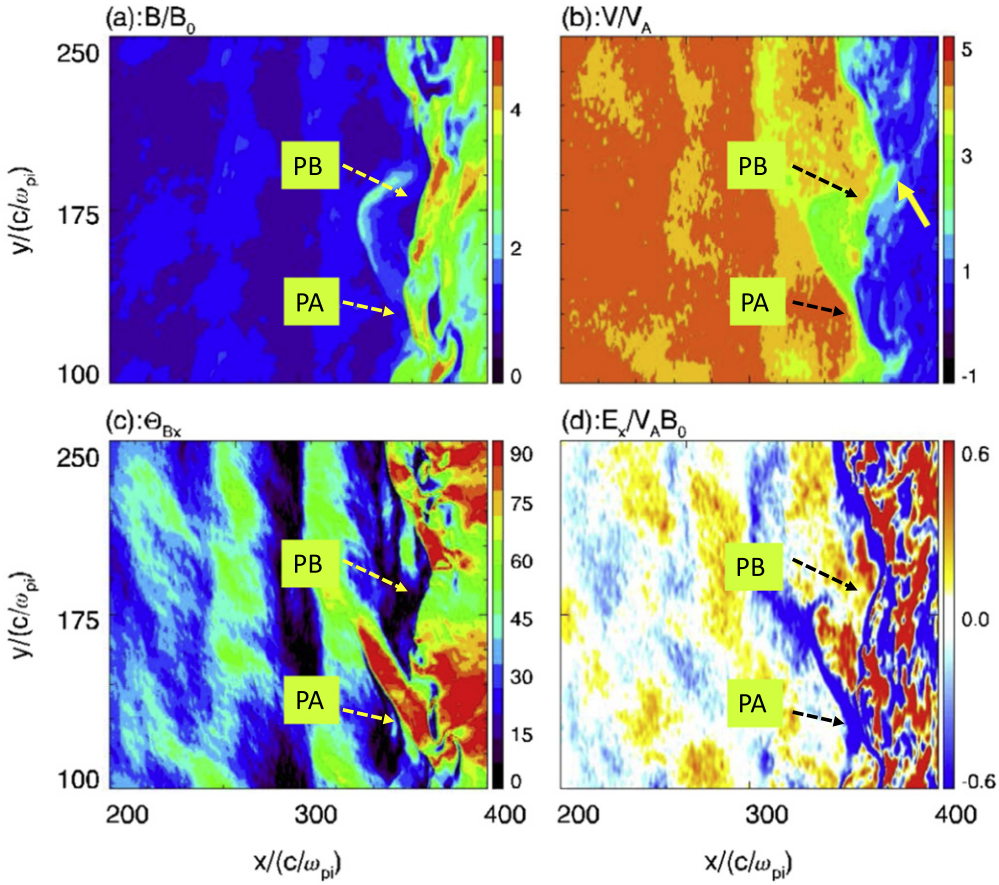

Figure 6. (a) The total magnetic field B/B_0, (b) the bulk velocity V/V_A, (c) the local angle between the magnetic field and the x direction θ_{Bx}, and (d) the electric field in the x direction E_x at $\Omega_i t = 121.5$, when the particles from regions "A" and "B" just begin to interact with the shock. Here "PA" and "PB" denote the lower and upper parts of a ripple. A yellow bold arrow in the upper right panel labels a high-speed jet downstream of the shock.

the ripple tends not only to reflect more upstream ions, but also to decelerate the transmitted ions more efficiently.

Because of the different characteristics of transmitted ions after the upstream ions interact with the different parts of a ripple at a quasi-parallel shock, the bulk velocities of these transmitted ions are different along the y direction; this leads to the formation of high-speed jets observed downstream of a quasi-parallel shock by *Cluster* (Hietala et al. 2009). In order to demonstrate the generation mechanism of the high-speed jets, in Figure 6 we plot (a) the total magnetic field B/B_0, (b) the bulk velocity V/V_A, (c) the local angle between the magnetic field and the x direction θ_{Bx}, and (d) the electric field in the x direction E_x at $\Omega_i t = 121.5$, when the particles from regions "A" and "B" just begin to interact with the shock. Here "PA" and "PB" denote the lower and upper parts of the ripple. A high-speed jet can be easily identified just downstream, corresponding to the upper part of the ripple, which is denoted by the yellow arrow in Figure 6(b). The bulk velocity of the particles in a high-speed jet is larger than that in the other downstream areas around it, and its size is about $15c/\omega_{\rm pi}$. In comparison with the lower part of the ripple (denoted by "PA"), θ_{Bx} is smaller and the electric field E_x is positive in the upper part of the ripple (denoted by "PB"), where the particles are decelerated with less efficiency when they are transmitted through the shock and lead to the formation of corresponding high-speed jets downstream.

In 1D hybrid simulations of a quasi-parallel shock, all superthermal ions come from upstream, where these particles are reflected by the shock and get accelerated when they are trapped between the old and new shock fronts until they escape upstream (Su et al. 2012a). Here, in 2D hybrid simulations of a quasi-parallel shock, superthermal ions come not only from upstream but also from downstream, as shown in Figure 4. In order to investigate the dynamics of these superthermal ions, we follow their trajectories, and find that there are four different categories. Figure 7 plots a typical ion trajectory of the first category. Figures 7(a)–(c) show the typical trajectory in the (x, y) plane at $\Omega_i t = 108.0$–143.0, 143.0–151.5, and 151.5–188.5, while 7(d) presents the evolution of its kinetic energy. The total magnetic fields at $\Omega_i t = 143.0$, $\Omega_i t = 151.5$, and $\Omega_i t = 180.0$ are overlaid in Figures 7(a)–(c) for reference. At $\Omega_i t = 108.0$, the particle is upstream and moves toward the shock. It is reflected by the shock at "A2," and then moves along the surface of the shock. At "A3," it leaves the shock and travels upstream, but it is trapped by a wave from the upstream region. The wave is steepening when approaching the shock front, and becomes a new shock front when it merges with the old one. At "A5," the particle again leaves the shock, and crosses the upstream waves when it goes further upstream. Note that here the particle crosses the lower boundary and will enter the simulation domain from the upper boundary due to the periodic boundary condition used in the simulation. The particle suffers acceleration in two stages: in the first stage (from "A2" to "A3"), the particle is reflected by the shock when approaching the shock front from upstream and moves along the shock surface; in the second stage (from "A3" to

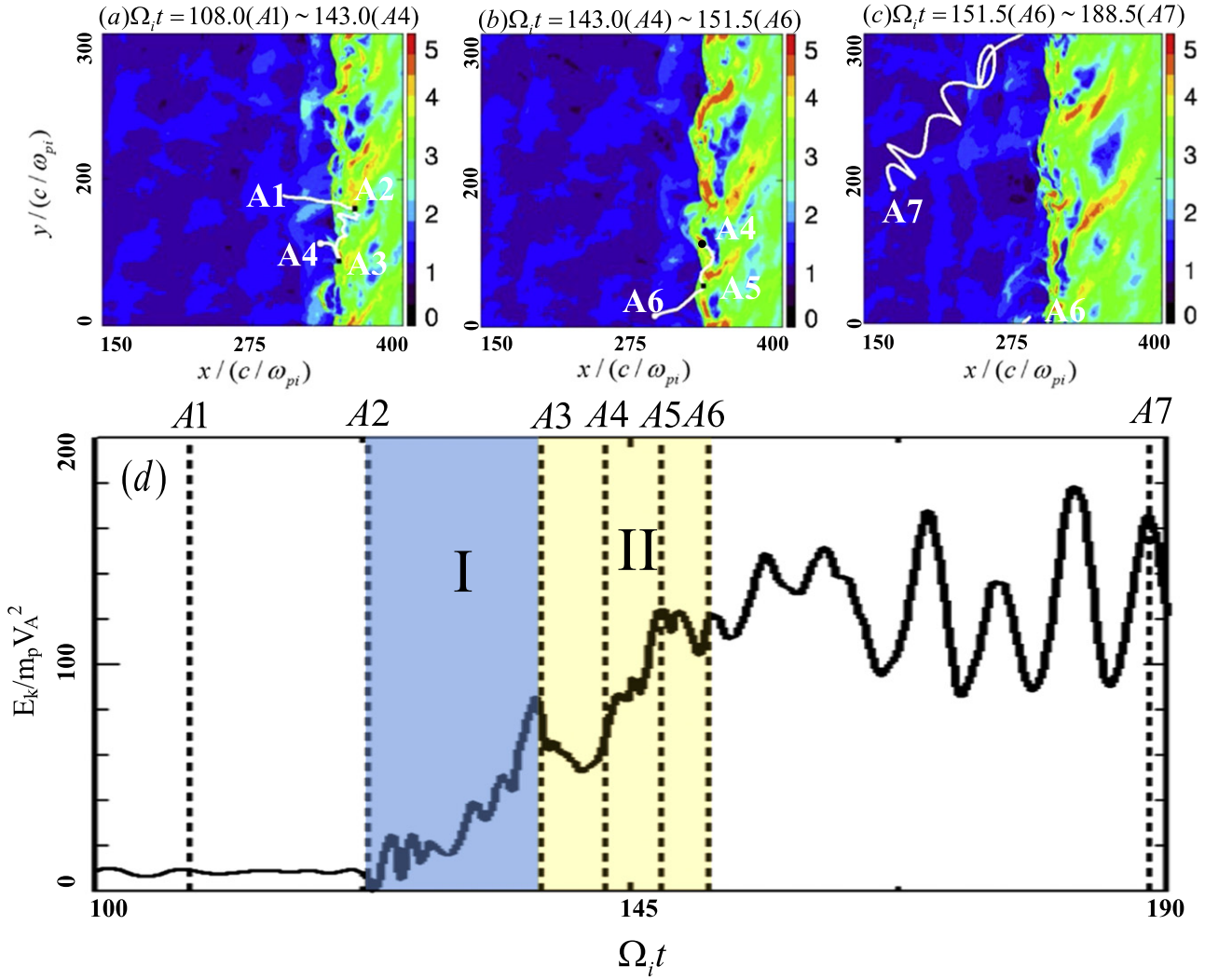

Figure 7. A typical ion trajectory of the first category. Panels (a)–(c) show the typical trajectory in the (x, y) plane at $\Omega_i t$ = 108.0–143.0, 143.0–151.5, and 151.5–188.5, while (d) presents the evolution of its kinetic energy. The total magnetic fields at $\Omega_i t$ = 143.0, $\Omega_i t$ = 151.5, and $\Omega_i t$ = 180.0 are overlaid in (a)–(c) for reference. The two areas denoted "I" and "II" show two stages of acceleration.

(An animation of this figure is available.)

"A5"), the particle is trapped between new and old shock fronts. The acceleration process is similar to that in a 1D quasi-parallel shock, which has been demonstrated clearly by Su et al. (2012a), except that now in 2D simulations the particle can move along the shock surface and escape easily to the upstream region due to the inhomogeneity of the shock front and upstream waves along the y direction.

Figure 8 plots a typical ion trajectory of the second category. Figures 8(a)–(c) show the typical trajectory in the (x, y) plane at $\Omega_i t$ = 110.5–140.5, 140.5–149.5, and 149.5–174.5, while 8(d) presents the evolution of its kinetic energy. The total magnetic fields at $\Omega_i t$ = 140.5, $\Omega_i t$ = 149.5, and $\Omega_i t$ = 174.5 are overlaid in Figures 8(a)–(c) for reference. The particle from upstream is reflected by the shock, and then it is accelerated when moving along the shock surface and trapped between the new and old shock fronts. However, unlike the particles from the first category, the particle finally enters the downstream region after crossing the shock front where the magnetic field is weak.

Figure 9 plots a typical ion trajectory of the third category. Figures 9(a)–(d) show the typical trajectory in the (x, y) plane at $\Omega_i t$ = 114.0–144.0, 144.0–158.0, 158.0–172.0, and 172.0–188.5, while 9(e) presents the evolution of its kinetic energy. The total magnetic fields at $\Omega_i t$ = 144.0, $\Omega_i t$ = 158.0, $\Omega_i t$ = 172.0, and $\Omega_i t$ = 188.5 are overlaid in Figures 8(a)–(d) for reference. After being reflected by the shock, the particle is accelerated when moving along the shock surface and trapped between the new and old shock fronts. However, after the particle escapes upstream, it can be trapped again by the wave further upstream and suffer an acceleration process of more than two stages. Finally, the particle may escape further upstream (see Figure 9), or cross the shock and travel downstream (see Figure 10, which plots a typical ion trajectory of the fourth category). Figures 10(a)–(d) show the typical trajectory in the (x, y) plane at $\Omega_i t$ = 112.5–142.5, 142.5–151.5, 151.5–165.5, and 165.0–188.5, while 10(e) presents the evolution of its kinetic energy. The total magnetic fields at $\Omega_i t$ = 142.5, $\Omega_i t$ = 151.5, $\Omega_i t$ = 165.5, and $\Omega_i t$ = 188.5 are overlaid in Figures 10(a)–(d) for reference. The particle finally

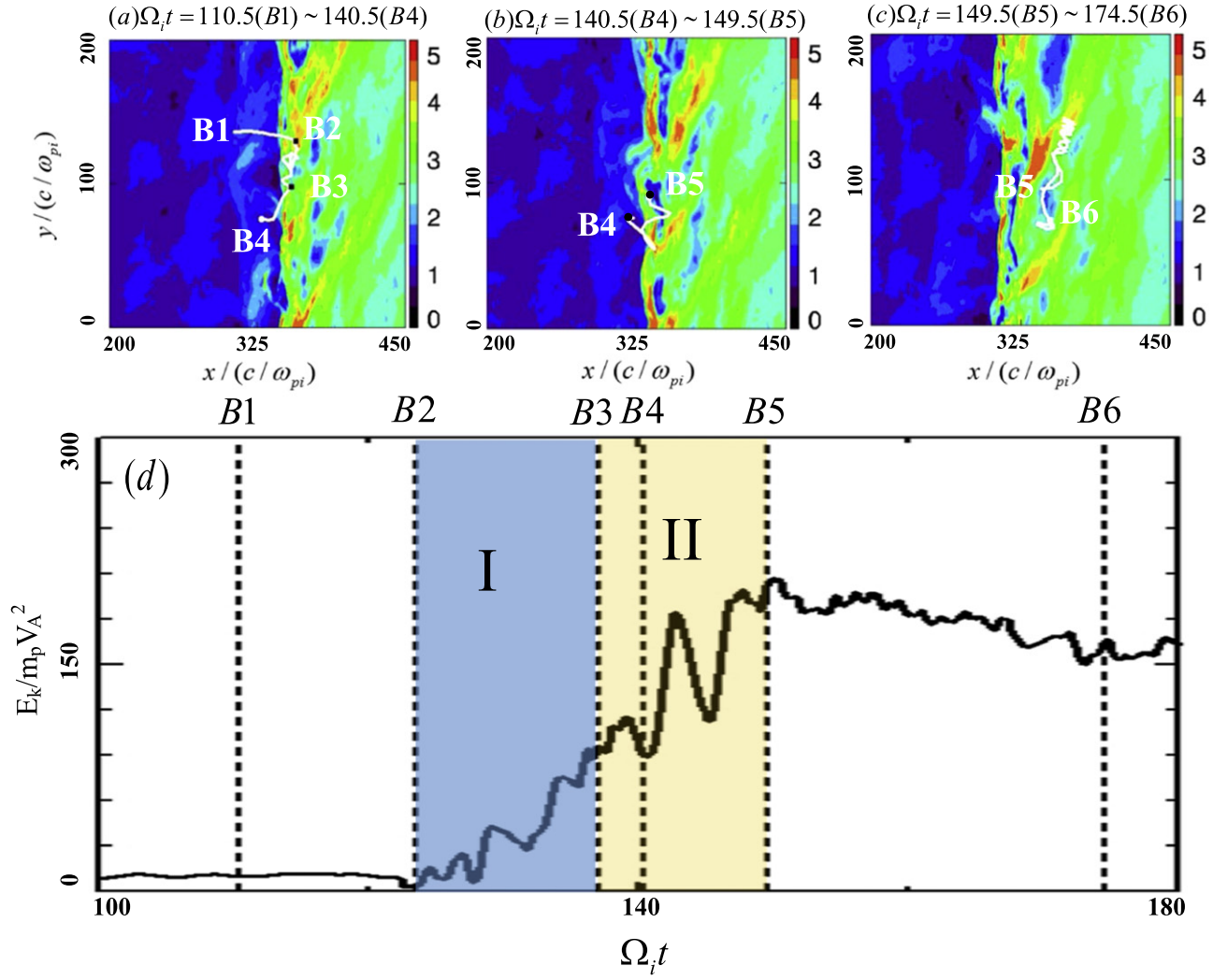

Figure 8. A typical ion trajectory of the second category. Panels (a)–(c) show the typical trajectory in the (x, y) plane at $\Omega_i t$ = 110.5–140.5, 140.5–149.5, and 149.5–174.5, while (d) presents the evolution of its kinetic energy. The total magnetic fields at $\Omega_i t$ = 140.5, $\Omega_i t$ = 149.5, and $\Omega_i t$ = 174.5 are overlaid in (a)–(c) for reference. The two areas denoted "I" and "II" show two stages of acceleration.

(An animation of this figure is available.)

travels downstream after it suffers an acceleration process of more than two stages.

In summary, the superthermal ions are those particles that are reflected by the shock and get accelerated when moving along the shock surface, and are then trapped between the upstream waves (or new shock front) and the shock front. Finally, those particles may escape further upstream or move downstream. Therefore, the superthermal ions can be found both upstream and downstream. About 20% of the superthermal ions are found downstream, and 30% suffer an acceleration process of more than two stages. In general, particles that suffer an acceleration process of more than two stages can be accelerated to much higher energy than those that undergo only two-stage acceleration; this means that the trapping in upstream waves and subsequent acceleration are more efficient than trapping in the new shock front alone. The importance of the upstream waves in the generation of seed particles for further DSA acceleration has already been emphasized with satellite observations (Wu et al. 2015; Johlander et al. 2016).

4. CONCLUSIONS AND DISCUSSION

In this paper, 2D hybrid simulations are performed to investigate the ion dynamics at a quasi-parallel shock. Obvious ripples are found to form around the shock front, and at the same time the shock is re-forming: a new shock front may appear in the upstream region, which is convected to the shock front by the upstream flow, and finally merges with the old shock front. However, the re-formation of the shock is not synchronous along the y direction due to the existence of the ripples. When the upstream ions interact with the quasi-parallel shock, their behaviors will be different in different y directions. The upstream ions tend to be reflected in the lower part of a ripple, while they are transmitted more easily through the upper part of a ripple. In the downstream region corresponding to the upper part of a ripple, the bulk velocity is larger, and then a high-speed jet is formed. Therefore, the observed high-speed jets downstream are the results of the ripples inherent in a quasi-parallel shock. High-speed jets have already been observed by satellites downstream of quasi-parallel shocks

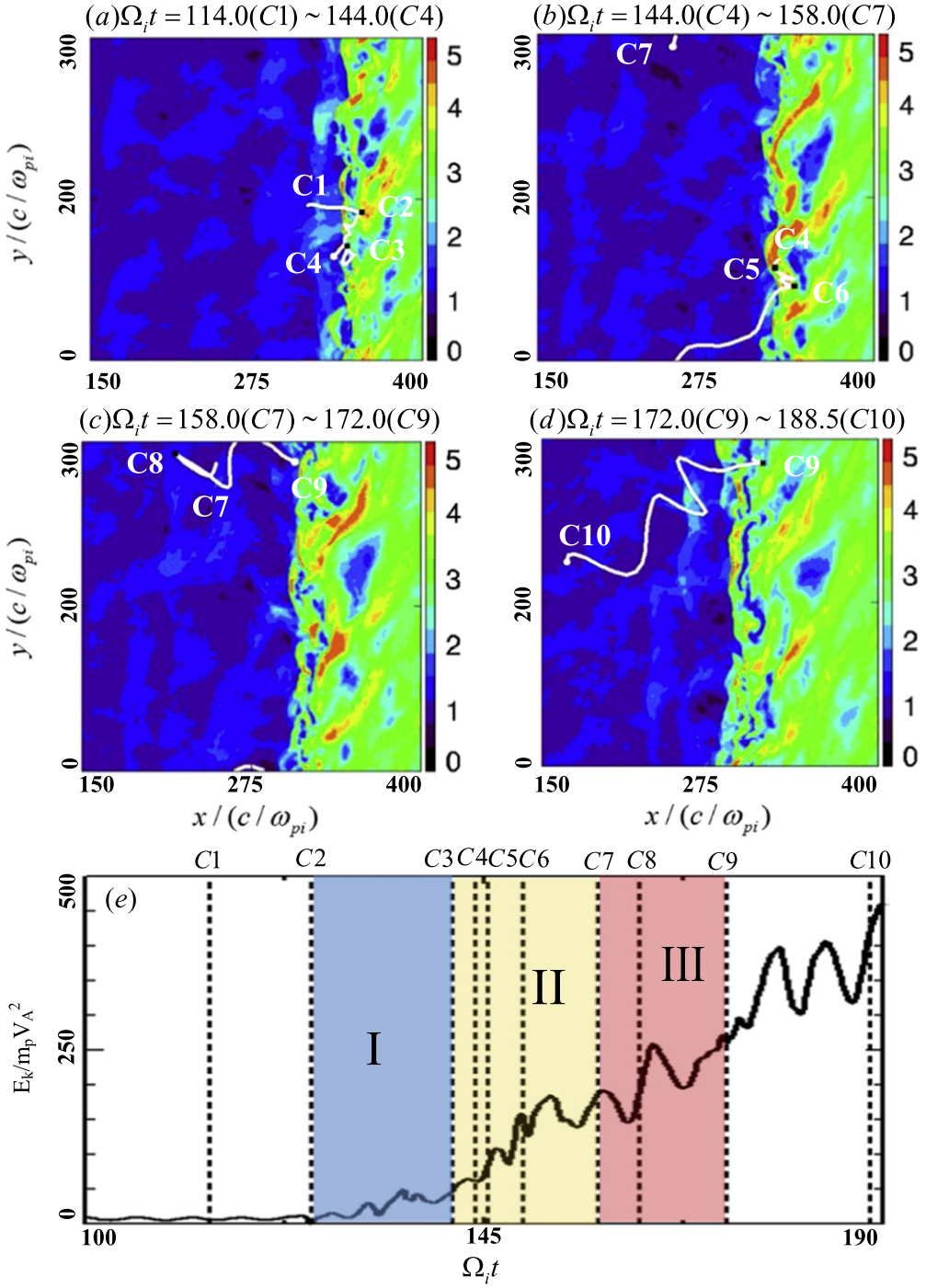

Figure 9. A typical ion trajectory of the third category. Panels (a)–(d) show the typical trajectory in the (x, y) plane at $\Omega_i t$ = 114.0–144.0, 145.0–158.0, 158.0–172.0, and 172.0–188.5, while (d) presents the evolution of its kinetic energy. The total magnetic fields at $\Omega_i t$ = 144.0, $\Omega_i t$ = 158.0, $\Omega_i t$ = 172.0, and $\Omega_i t$ = 188.5 are overlaid in (a)–(d) for reference. The three areas denoted "I," "II," and "III" show three stages of acceleration.

(An animation of this figure is available.)

(Němeček et al. 1998; Archer et al. 2012; Hietala et al. 2012; Plaschke et al. 2013). The upstream particles tend to be reflected by the shock in the lower part of a ripple. The ions reflected by the shock are accelerated when they move along the shock surface, or are trapped between the upstream waves (include the new shock front) and the shock front.

Particles accelerated by a shock through the DSA mechanism are considered to be an important source of the observed power-law spectra of energetic particles from cosmic rays to gradual solar energetic particle events. However, in order for the DSA mechanism to work in a shock, the energy of the particles must exceed a threshold, or the particles need at first to be pre-accelerated to become superthermal particles. The acceleration of the reflected particles by a shock is considered to provide such a pre-acceleration mechanism. In 1D simulations of a quasi-parallel shock, the reflected ions are accelerated when they are trapped between the new and old shock fronts during the re-formation of the shock. These particles escape from the shock to

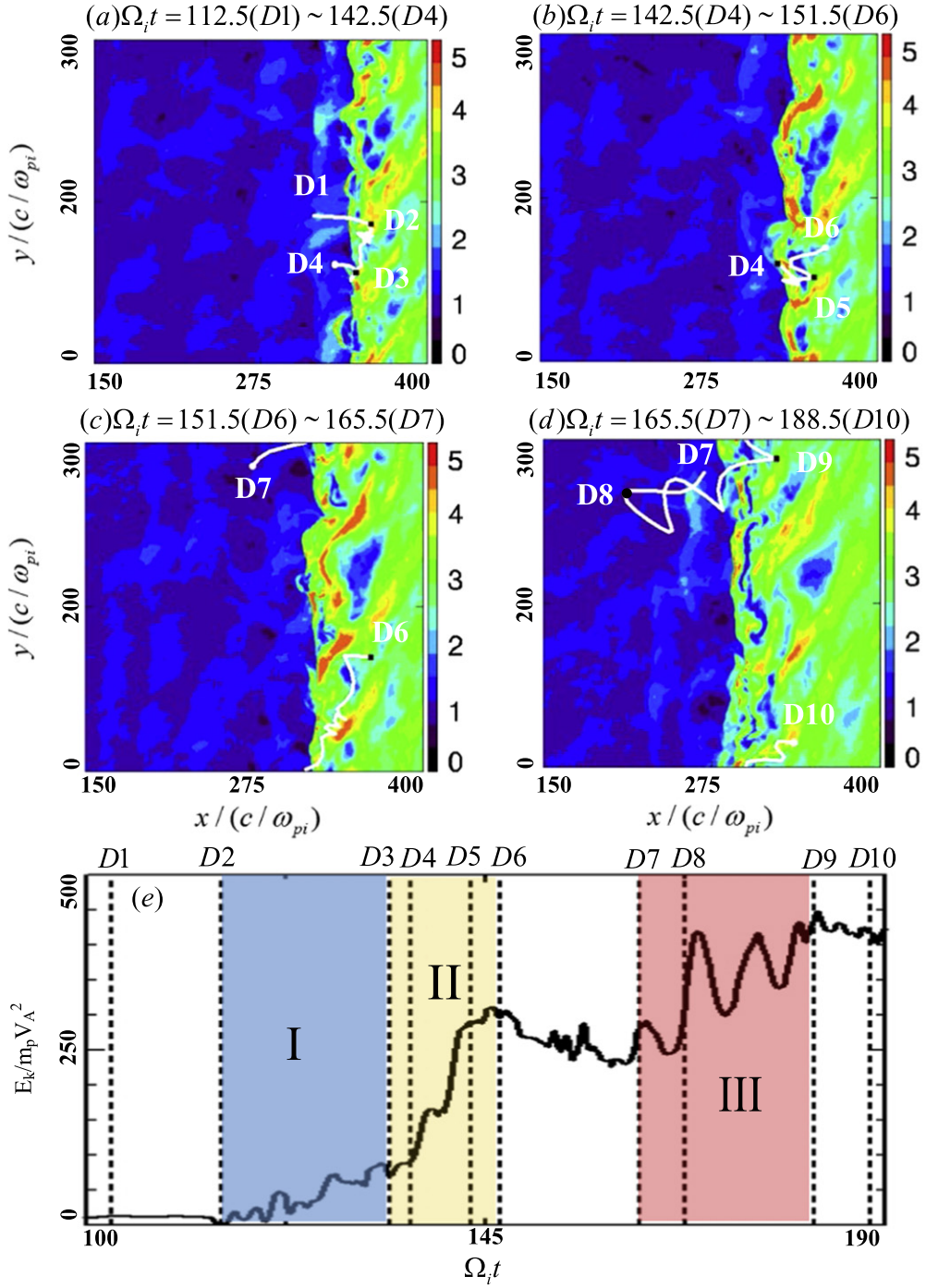

Figure 10. A typical ion trajectory of the fourth category. Panels (a)–(d) show the typical trajectory in the (x, y) plane at $\Omega_i t$ = 112.5–142.5, 142.5–151.5, 151.5–165.5, and 165.5–188.5, while (d) presents the evolution of its kinetic energy. The total magnetic fields at $\Omega_i t$ = 142.5, $\Omega_i t$ = 151.5, $\Omega_i t$ = 165.5, and $\Omega_i t$ = 188.5 are overlaid in (a)–(d) for reference. The three areas denoted "I," "II," and "III" show three stages of acceleration.

(An animation of this figure is available.)

the upstream region after the cycle of re-formation is finished, and the superthermal ions can only be found upstream (Su et al. 2012a). Here, in 2D simulations of a quasi-parallel shock, because of the inhomogeneity of the shock front and upstream waves along the y direction, the reflected ions may leak upstream or downstream when they are trapped between the old and new shock fronts. The particles that leak upstream may be accelerated again by interaction with the upstream waves. The superthermal ions can be found both upstream and downstream, and they may suffer acceleration in several stages.

This work was supported by the National Science Foundation of China, grant Nos. 41331067, 11235009, 41527804, 41474125, 41421063, 973 Program (2012CB825602, 2013CBA01503).

REFERENCES

Archer, M. O., Horbury, T. S., & Eastwood, J. P. 2012, JGR, 117, A05228
Axford, W. I., Lee, E., & Skadron, G. 1977, ICRC, 11, 132
Bell, A. R. 1978, MNRAS, 182, 147
Blanco-Cano, X., Kajdič, P., Omidi, N., & Russell, C. T. 2011, JGR, 116, A09101
Blanco-Cano, X., Omidi, N., & Russell, C. T. 2009, JGR, 114, A01216
Blandford, R. D., & Ostriker, J. P. 1978, ApJL, 221, L29
Burgess, D. 1989, GeoRL, 16, 345
Burgess, D., Lucek, E. A., Scholer, M., et al. 2005, SSRv, 118, 205
Caprioli, D., PoP, A., & Spitkovsky, A. 2015, ApJL, 798, L28
Cui, Y. Q., Sheng, Z. M., Lu, Q. M., Li, Y. T., & Zhang, J. 2015, SCPMA, 58, 105201
Eastwood, J. P., Balogh, A., Lucek, E. A., Mazelle, C., & Dandouras, I. 2005a, JGR, 110, A11219
Eastwood, J. P., Balogh, A., Mazelle, C., Dandouras, I., & Reme, H. 2004, GeoRL, 31, L04804
Eastwood, J. P., Balogh, A., Lucek, E. A., Mazelle, C., & Dandouras, I. 2005b, JGR, 110, A11220
Fairfield, D. H. 1969, JGRA, 74, 3541
Gary, S. P., Smith, C. W., Lee, M. A., Goldstein, M. L., & Forslund, D. W. 1984, PhFl, 27, 1852
Giacalone, J. 2003, ApJ, 609, 452
Guo, F., & Giacalone, J. 2013, ApJ, 773, 158
Hietala, H., & Plaschke, F. 2013, JGR, 118, 7237
Hietala, H., Laitinen, T. V., Andréeová, D., et al. 2009, PhRvL, 103, 245001
Hietala, H., Partamies, N., Laitinen, T. V., et al. 2012, AnGp, 30, 33
Johlander, A., Vaivads, A., Khotyaintsev, Yu. V., Retino, A., & Dandouras, I. 2016, ApJL, 817, L4
Jokipii, J. R. 1987, ApJ, 313, 842
Jones, F. C., & Ellison, D. C. 1991, SSRv, 58, 259
Kucharek, H., & Scholer, M. 1991, JGR, 96, 21195
Lee, M. A. 1983, JGR, 88, 6109
Li, G., Zank, G. P., & Rice, W. K. M. 2003, JGR, 108, 1082
Lin, Y. 2003, JGR, 108, 1390
Lucek, E. A., Horbury, T. S., Dandouras, I., & Rème, H. 2008, JGR, 113, A07S02
Němeček, Z., Šafránková, J., Přech, L., et al. 1998, GeoRL, 25, 1273
Omidi, N., Zhang, H., Sibeck, D., & Turner, D. 2013, JGR, 118, 173
Plaschke, F., Hietala, H., & Angelopoulos, V. 2013, AnGp, 31, 1877
Russell, C. T., & Hoppe, M. 1983, SSRv, 34, 155
Savin, S., Amata, E., Zelenyi, L., et al. 2012, AnGp, 30, 1
Scholer, M. 1990, GeoRL, 17, 1821
Scholer, M. 1993, JGR, 98, 47
Scholer, M., & Burgess, D. 1992, JGR, 97, 8319
Scholer, M., Fujimoto, M., & Kucharek, H. 1993, JGR, 98, 18971
Scholer, M., Kucharek, H., & Kato, C. 2002, PhPl, 9, 4293
Schwartz, S. J., & Burgess, D. 1991, GeoRL, 18, 373
Schwartz, S. J., Burgess, D., Wilkinson, W. P., et al. 1992, JGR, 97, 4209
Su, Y., Lu, Q., Gao, X., Huang, C., & Wang, S. 2012a, PhPl, 19, 092108
Su, Y., Lu, Q., Huang, C., et al. 2012b, JGR, 117, A08107
Thomas, V. A., Winske, D., & Omidi, N. 1990, JGR, 95, 18809
Wilson, L. B., III, Koval, A., Sibeck, D. G., et al. 2013, JGR, 118, 957
Winske, D. 1985, SSRv, 42, 53
Winske, D., Omidi, N., Quest, K. B., & Thomas, V. A. 1990, JGR, 95, 821
Wu, M., Hao, Y., Lu, Q., et al. 2015, ApJ, 808, 2
Zank, G. P., Rice, W. K. M., le Rous, J. A., Cairns, I. H., & Webb, G. M. 2001, PhPl, 8, 4560
Zank, G. P., Rice, W. K. M., & Wu, C. C. 2000, JGR, 105, 25079
Zuo, P. B., Zhang, M., & Rassoul, H. K. 2013, ApJ, 767, 6